SMART Cable Sensors: Requirements Update 2025

Sensor Review Working Group
of the
Joint Task Force on SMART Cables

August 2025

Preface

SMART Cables are commercial submarine telecommunications cables that have environmental sensors for climate and disaster risk reduction. SMART stands for Science Monitoring And Reliable Telecommunications.

This report provides an updated review of SMART Cable sensor use cases, performance requirements/specifications and recommendations. The sensors considered are for ocean bottom temperature, pressure and seismic motion.

It builds upon and is complementary to sensor performance sections in two earlier reports: Functional requirements of "green" submarine cable systems, 2015; and General Requirements for Sensor Enabled And Reliable Telecommunications (SMART) Cable Systems, 2016; as well as descriptions of science enabled by SMART Cables in three recent papers—SMART Cables for Observing the Global Ocean: Science and Implementation, 2019; SMART Subsea Cables for Observing the Earth and Ocean, Mitigating Environmental Hazards, and Supporting the Blue Economy, 2022; and SMART Cables Observing the Oceans and Earth, 2022.

This report was prepared and written by the JTF Sensor Review Working Group (SRWG; below) led by Laura Wallace (temperature and pressure) and William Wilcock (seismic) with support of the SMART Cables International Programme Office.

Bruce Howe
Chair, JTF SMART Cables
26 August 2025

Acknowledgements:
The Joint Task Force for SMART Cables is a volunteer effort sponsored by the International Telecommunications Union, World Meteorological Organization, and UNESCO Intergovernmental Commission (ITU/WMO/UNESCO-IOC). The work of the JTF is coordinated through its International Programme Office, with generous support from the Gordon and Betty Moore Foundation and Schmidt Marine Technology Partners, to whom we extend our gratitude. This report was made possible thanks to the dedication and contributions of the members of the Sensor Review Working Group (SRWG), who serve as part of the JTF community.

Citation:
JTF SMART Cables Sensor Review Working Group, SMART Cable Sensors: Requirements Update, 2025.

JTF SMART Cables Sensor Review Working Group

Co-Leads:
Laura Wallace, GEOMAR, and William Wilcock, University of Washington

Members:

Shima Abadi, University of Washington
Jean Paul Ampuero, GeoAzur
Keisuke Ariyoshi, JAMSTEC
Joerg Bialas, GEOMAR
Paul Bodin, University of Washington
Peter Brandt, GEOMAR
Fernando Carrilho, IPMA
Emmy Tsuiyu Chang, National Taiwan University
Carlos Corela, Inst. Dom Luiz
Matt Fouch, Subsea Data Systems
Chris Hughes, University of Liverpool
Helen Janiszewski, University of Hawaii
Greg Johnson, RBR
Marián Jusko, Nanometrics
Patanjali Kumar Chodavarapu, INCOIS
Michel LeBlanc, Halliburton
James Lindsey, Guralp Systems
Brad Lipovsky, University of Washington
Francisco López Torres, Aragon Photonics Labs
Nadim Mahmud, Bangladesh Weather Observation Team
Hiroyuki Matsumoto, JAMSTEC
Pierre Mertz, Infinera
Mikael Mazur, Nokia
Aldo Monaca, Oceans and Cables
Laurence Moskowitz, Global Broadband Solutions
Teresa Nick, Microsoft
Eric Rehm, Sea-Bird Scientific
Will Reis, Sonardyne International
Veronica Rodriguez Tribaldos, GFZ Potsdam
Masanao Shinohara, University of Tokyo
Anthony Sladen, GeoAzur
Frederik Tilmann, GFZ Potsdam
Arantza Ugalde, Institute of Marine Sciences, CSIC
Krishna Venkateswara, Paroscientific
Joao Vitorino, Portugal Instituto Hidrografico
Spahr Webb, Columbia University
Zhongwen Zhan, Caltech
Natalie Zielinski, Sea-Bird Scientific
Tatsuya Kubota, National Research Institute for Earth Science and Disaster Resilience
Amy Williamson, Berkeley Seismological Laboratory

Table of Contents

SMART Cable Specifications and Recommendations for Temperature Sensors

Temperature variations within the ocean have a profound impact on ocean circulation processes. Like pressure, temperature is classified as an Essential Ocean Variable (https://goosocean.org/what-we-do/framework/essential-ocean-variables/). Moreover, temperature changes in the oceans result in thermal expansion, thus influencing sea level change. In our rapidly changing climate, it is becoming increasingly important to monitor changes in temperature within the oceans, inform heat storage within the oceans, and quantify the influence of this on ocean circulation and sea level change. Continuous temperature sensing as part of a SMART cable system can be used for the following:

(1) Quantify heat storage in the oceans, thermal expansion, and impact on sea level rise;
(2) Coastal upwelling and shelf exchange processes;
(3) Mixing in the bottom boundary layer; and
(4) Detect submarine sediment transport processes (e.g., turbidity currents).

It is important to consider the placement of temperature sensors in SMART sensor packages on telecommunications cables. For example, if the sensors are co-located with the telecommunications repeater, then the heat source of the repeater can adversely affect the temperature measurements being made. Thus, if temperature measurements are of critical importance, sensor pods/packages should be housed separately from the repeater and positioned at a sufficient distance away from the repeater such that the temperature measurements are not influenced by the presence of the repeater.

Quantify heat storage in the oceans, thermal expansion, and impact on sea level rise

The oceans take up most of the heat excess on Earth and thermal expansion as the oceans warm is an important contributor to sea level rise. Bottom temperature measurements in the deep ocean would allow us to address the warming of bottom waters in the global ocean. During recent decades, a warming of the Antarctic Bottom Water that affected all the major ocean basins was observed. These decadal changes substantially contribute to global energy and sea level budgets (Purkey and Johnson, 2010). Observed decadal changes in the deep ocean are of the order of 10^{-3} °C (e.g., Herrford et al., 2017; Zhou et al., 2023).

Coastal upwelling and shelf exchange processes

Bottom temperature variability at the continental slope and shelf is impacted by upwelling and downwelling processes associated with local wind forcing or remotely generated boundary waves. Temperature variation can be large (~1 °C) in the depth range of the main or seasonal thermocline. Such temperature fluctuations associated with upwelling events occur on timescales from days to seasonal, impacting upward nutrient supply and marine ecosystems (Körner et al., 2024).

Mixing in the bottom boundary layer

Temperature fluctuations and variability on the seafloor are an indicator of stirring and mixing associated with the bottom boundary layer, ultimately reaching into the ocean interior. There are very few deep ocean bottom temperature long time series observations. Currently, there are several extant time series. These include measurements at Station ALOHA from the ALOHA Cabled Observatory and the Woods Hole Oceanographic Institution (WHOI) Hawaii Ocean Timeseries (HOT) Site (WHOTS). In the last 14 years, data from these sites show rapid changes, as much as 40 mK in a day (peak-to-peak), with slow recovery on time scales of half a year (https://aco-ssds.soest.hawaii.edu/dataDisplay.php). Temperature measurements in the Northwestern Argentine Basin (Meinen et al., 2020) and deep ocean off Chile at 21 ºN on each side (not in) of the trench (Jegen et al., 2024) show similar levels of variability, although with differing structure. Similar fluctuations are found at the Stratus Ocean Reference Station (ORS) off Chile and the Northwest Tropical Atlantic Station (NTAS). These two, with WHOTS, paired CTDs just at the anchor as part of the "Deep Ocean Observing Challenge".

The inherently sparse existing observations suggest that the deep ocean is not quiescent and high-frequency, long-term temperature observations on SMART sensors will inform the quantification of ocean mixing.

Submarine sediment transport processes

Turbulent submarine sediment-laden gravity flows, known as turbidites, are an important type of sediment mass transport in the oceans. As these flows transport warmer water from shallower depths into deeper depths, they can produce detectable temperature changes as they pass (e.g., Arai et al., 2013; Johnson et al., 2017). Seafloor temperature data can be used in conjunction with pressure data to detect such flows to better understand the occurrence, distribution, magnitude, and frequency of these phenomena.For example, a temperature and pressure anomaly observed on an Ocean Bottom Pressure gauge following the 2011 Tohoku-Oki M9 earthquake was shown to be due to a turbidite generated by the earthquake (Arai et al., 2013). Seafloor temperature changes due to passing turbidite flows can be on the order of 0.5–0.01°C and have durations of hours (Arai et al., 2013) to days/months (Johnson et al., 2017).

Table 1. Temperature sensing requirements for the different applications discussed.

Application	Heat storage/sea level rise	Coastal shelf exchange processes	Mixing in the boundary layer	Submarine sediment transport
Resolution	0.0001 °C	0.1 °C	0.0001 °C	≤0.01°C
Stability	≤0.002 °C/yr	≤0.002 °C/yr	≤0.002 °C/yr	≤0.005 °C/yr
Sample rate	0.1 Hz	1 minute	1 Hz	1 Hz
Duration of signals observed	years to decades	hours to years	seconds to decades	minutes to weeks

SMART Cable Specifications and Recommendations for Pressure Sensors

Ocean bottom pressure sensors can detect small changes in water pressure at the seafloor, which are produced by variations in the height and density of the overlying water column. Pressure sensors installed as part of SMART sensing packages on telecommunications cables have several primary uses.

(1) Detect seafloor pressure changes due to passing tsunami waves. These data can be used for early tsunami warnings (Bernard et al., 2014) and scientific investigations of tsunami generation and propagation processes.

(2) Detect mass change within the oceans (e.g., from melting land ice) with implications for global sea level budgets (Hughes et al., 2012; Williams et al., 2014).

(3) Investigate global and regional ocean circulation variability associated with general circulation (e.g., across ocean basins, such as the Atlantic Meridional Overturning Circulation), planetary waves, topographically trapped waves, eddies, tides, and internal waves (Ray, 2013; Hughes et al., 2018). The pressure gradient between two points is typically used to infer the flow.

(4) Detect vertical displacement of the seabed in earthquakes (e.g., Iinuma et al., 2012) and/or transient deformation events that produce cm-level, or larger, vertical displacements (e.g., as slow slip events or volcano deformation events; Chadwick et al., 2006; Wallace et al., 2016).

(5) Seismic sensor that will not clip on signals from any seismic event, complementing a strong motion vertical seismometer (Webb and Nooner, 2016) to observe P waves and Rayleigh waves (e.g., Matsumoto et al., 2018; Tréhu et al., 2020).

(6) Sensor that can be used to correct the vertical channel of broadband seismometers at long periods for compliance noise arising from the deformation of the seafloor under surface infragravity waves (Webb and Crawford, 2010, Bell et al., 2015).

(7) Detect submarine sediment transport processes (such as turbidity currents; Arai et al., 2013; Johnson et al., 2017).

(8) Component of the Global Geodetic Observing System to constrain geocenter motion and Earth rotation variations, which are relevant for a wide variety of satellite and navigation systems.

Most high-resolution ocean bottom pressure measurements are undertaken with Absolute Pressure Gauges (APGs) based on a vibrating quartz resonator transducer (e.g., Houston and Paros, 1998). One of the well-known limitations of standard APGs (particularly for some oceanographic and seafloor geodetic applications—see items 2–4 above) is that they drift on the order of several cm/yr equivalent water depth (Polster et al., 2009). This drift introduces a large source of uncertainty in the use of seafloor pressure data to resolve long-term oceanographic changes (such as sea level rise of 5–10 mm/y) and long-term vertical tectonic changes. Without drift correction, APGs are only reliable for observing seafloor pressure changes that last less than a few months.

Recently, new methods were developed to quantify and correct for APG sensor drift (known as Ambient-Zero-Ambient, or A-0-A), successfully reducing drift in some cases to <1 cm/yr (Wilcock et al., 2021; Woods et al., 2022). Such drift-corrected sensors should be incorporated into SMART sensor packages, as this will enable important applications of seafloor pressure sensor data, including: (1) evaluation of long-term oceanographic changes (e.g., longer than a few months); and (2) evaluation of secular vertical deformation due to a range of long-term tectonic and geodynamic processes, including glacio-isostatic rebound and earthquake cycle deformation processes (such as interseismic elastic strain accumulation on offshore faults). For the DONET cabled network offshore southwest Japan, standard APG sensors (without A-0-A) stability and drift characteristics were also screened prior to their deployment by pressurizing the sensors for one month using a deadweight tester (Matsumoto and Araki, 2021). This could also be undertaken when using standard APGs in order to select sensors with lower rates of drift although, unlike A-0-A, this does not provide a means to remove drift altogether.

There are also recent evolving developments in silicon resonant-type pressure sensors based on the MEMS technology, which are now being used as tsunami sensors in the Nankai Trough Seafloor Observation Network for Earthquakes and Tsunamis (N-net) in Japan (e.g., Aoi et al., 2020). The offshore N-net system was installed in early 2024, followed by the near-shore system in early 2025. In the meantime, a tsunami from the moderate-to-strong earthquake with magnitude 7.1 on 8 August 2024 was first recorded by the N-net pressure sensors (Kubota et al., 2025). Additionally, the Japan Meteorological Agency (JMA) has started using the offshore N-net pressure data for real-time tsunami warning in 2024. The drift characteristics of this new silicon resonant-type pressure sensor are not yet known. Depending on the performance of these new pressure sensors being deployed on N-net, this could be another option to consider in the future.

Requirements for sample rates, resolution, noise levels, and other specifications will vary depending on the application of the pressure data. Below, we outline the potential applications of seafloor pressure data and observational requirements. The Global Ocean Observing System (GOOS) designated ocean bottom pressure an Essential Ocean Variable (EOV); the associated specification sheet also provides a useful summary of the value of seafloor pressure data for a range of applications (https://goosocean.org/document/32488).

Tsunami early warning and tsunami generation/propagation processes

Seafloor pressure data enable detection and quantification of the amplitude of passing tsunami waves, and is one of the primary means of detecting and forecasting tsunamis. Currently, DART buoy networks around the world use moored buoys to convey seafloor pressure sensor data to the surface (via an acoustic modem) and onward transmission of the data to tsunami warning centers via satellite. Such data can give hours of advance warning of an approaching tsunami (particularly for distant or regional sources). A more comprehensive global network of pressure sensors on SMART cables would transform our ability to detect and more accurately forecast tsunamis. A global network of pressure sensors on SMART cables (which do not require regular maintenance) would represent a large cost-savings compared to the DART buoy network, which require frequent visits to maintain and replace the sensors and other infrastructure.

Beyond the immediate early warning and tsunami forecasting needs, seafloor pressure data are necessary to understand the source of tsunamis, as well as the geophysical and hydrodynamic processes that influence tsunami generation and propagation in the ocean basins and coastal regions. Seafloor pressure data from outside the source region are typically used as an input to a tsunami propagation model. Seafloor pressure data provide critical pieces of information to characterize the source of the tsunami, such as an earthquake, landslide, or volcanic eruption (e.g., Fukao et al., 2018). These data also reveal how tsunami waves travel in the world's ocean basins and how such deep ocean waves propagate into coastal regions to produce deadly tsunami waves (e.g., Maeda et al., 2011; Kubo et al., 2022; Fujii and Satake, 2024).

For pressure data from outside the source region to be useful for tsunami forecasting and scientific purposes, a minimum of one sample per minute is needed, although 1 Hz is preferable. As tsunami wave amplitudes in the open ocean can be <1 cm, the sensor should be able to reliably sense pressure changes of 10–100 Pa (equivalent to 1–10 mm of water column height) over periods of seconds to hours. Pressure observations from within the source region of an earthquake may contribute to characterization of the vertical displacement of the seafloor, thus contributing to more rapid and accurate characterization of the tsunami source if this crustal deformation signal can be untangled from the large reverberation signal. Within the source region, pressure changes due to earthquake signals can be very large but these can be reliably measured with absolute pressure gauges because of their large dynamic range. However, this requires a high sampling rate of at least 40 Hz (e.g., Nosov and Kolesov, 2007; Webb and Nooner, 2016).

Ocean Mass Change and Global Sea level budgets

Seafloor pressure provides a measure of ocean mass variability. In tandem with other types of datasets (such as satellite altimetry measurements of absolute sea level change), it can provide a highly useful measure of mass change in the oceans. This is highly complementary to Gravity Recovery and Climate Experiment (GRACE) satellite measurements and sea floor pressure data can provide higher resolution (spatially and temporally, unaliased in time) measurements of mass change, which can be used to validate GRACE measurements. In order to harness the power of ocean bottom pressure measurements to detect long-term (interannual to decadal) changes in ocean mass and the contribution of this to global sea level budgets, however, pressure sensor drift must be overcome. This sets forth an important challenge to reduce the sensor drift using A-0-A (or other techniques) as much as possible (e.g., ideally to less than a few mm/yr, which is not possible with current A-0-A systems). Even without drift correction, the measurements can provide strong constraints on ocean mass variability and help to fill in the missing geocenter information needed by satellites to monitor global ocean mass changes.

Investigate global and regional ocean circulation processes

Seafloor pressure provides important constraints on ocean circulation (Ray, 2013; Hughes et al., 2018). Continuous measurements of ocean bottom pressure at arrays of sites constrains oceanographic variability on multiple timescales (minutes to decades), including internal tides, infragravity waves, eddies, boundary waves, and ocean currents such as the Atlantic meridional overturning circulation (AMOC) as a major element of the Earth climate system. Bottom pressure data can also be utilized to constrain and validate Ocean Global Circulation Models. To investigate the AMOC (and possible spatio-temporal changes), seafloor pressure data are particularly important along the continental slope to resolve the depth structure of the overturning circulation. Such measurements allow a zonally integrated view of the meridional transport of mass and heat as part of the AMOC from seasonal to decadal time scales (Hughes et al., 2018; Herrford et al., 2021). At the same time, such measurements allow a quantification of boundary waves on subseasonal (e.g., wind-driven) to seasonal time scales, which may have local impacts on processes such as coastal upwelling, upward nutrient supply and marine ecosystems (Körner et al., 2024), and communicate causes of coastal sea level change from distant regions of the ocean

Measuring Vertical Displacement of the Seafloor (seafloor geodesy)

Continuous measurements of seafloor pressure change are becoming increasingly widely used as a seafloor geodetic tool to measure vertical seafloor displacement. If the seafloor uplifts, a pressure decrease will be recorded and, conversely, if the seafloor subsides, a pressure increase will be recorded. This concept is used to detect the distribution of vertical deformation of the seabed from earthquakes (Iinuma et al., 2012), magma transport at volcanic centers (Chadwick et al., 2006), and during slow slip events (slow-motion earthquakes lasting weeks to months) (Wallace et al., 2016; Woods et al., 2022). Seafloor pressure measurements are capable of resolving cm-level (or larger) vertical seabed displacements during events lasting seconds (earthquakes) to several weeks (slow slip events). These measurements provide crucial data on surface deformation to enable resolution of the distribution and magnitude of slip in offshore earthquakes and slow slip events at subduction zones and other types of plate boundaries, and monitor volcanic processes in offshore environments. Such data are rare and increasingly important for understanding the geohazards posed by offshore plate boundaries.

If pressure sensor drift can be mitigated using methods such as A-0-A, this opens up a wider scope of applications for seafloor geodesy. If drift can be reduced to <1–2 cm/yr (and preferably better), then it becomes possible to detect long-term vertical displacements due to tectonic, volcanic, and other processes. For example, vertical deformation rates are a diagnostic indicator of interseismic locking and stress accumulation on subduction plate boundary faults (Aoki and Scholz, 2003), and would enable identification of where stress is building prior to large megathrust earthquakes. Drift corrected pressure would also provide a valuable means of quantifying glacio-isostatic rebound beneath the oceans, which is an important component to consider in future sea level change projections (e.g., Peltier, 1999).

This in turn would improve the interpretation of satellite gravity measurements of global mass redistribution.

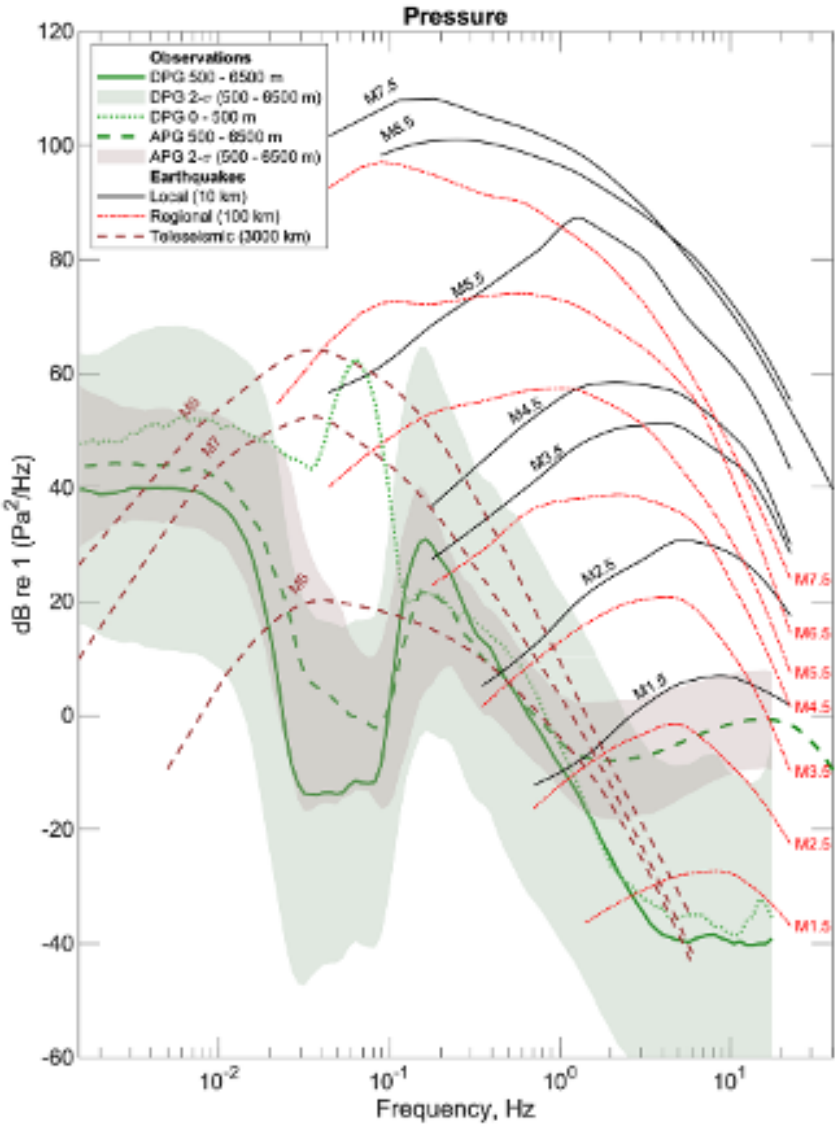

Figure 1. Pressure noise spectra compared with the peak pressure amplitudes of typical earthquakes. Noise spectra from the compilation of Janiszewski et al. (2023) show the mean and two standard deviation limits at depths of 500–6500 m (solid green line and light green shading) and the mean at depths 0–500 m (dotted green) for differential pressure gauge data, and the mean and two standard deviation limits at depths of 500–6500 m (dashed green and tan shading) for Paroscientific absolute pressure gauges. Note that the standard deviations for differential pressure gauges have a wide bound because of problems with some instrument calibration coefficients. Peak pressures for earthquakes are from Clinton and Heaton (2002) and show local earthquakes at 10 km distance (red dot-dashed), regional earthquakes at 100 km (black solid) and teleseismic earthquakes at 1000 km (brown dashed) for various magnitudes.

Seismology

One of the advantages of APGs is their large dynamic range (equivalent to the water column depth). This contrasts with most types of seismometers, whose measurements "clip" during very large events. It is long-known that hydrodynamic pressure at the seafloor induced by an earthquake is proportional to the vertical ground motion (Filloux, 1983). Thus, if ocean bottom pressure measurements are sampled at a sufficiently high rate (≥ 40 Hz) they can be used to augment data from vertical component seismometers, which is particularly valuable during large, local events (e.g., Tréhu et al., 2020; Webb and Nooner, 2016) (Figure 1). Webb and Nooner (2016) introduced a new method of counting during pressure sensor logging that minimizes the aliasing of higher-frequency counting noise, which produces a large improvement in the resolution of pressure measurements. Utilizing such logging approaches is recommended, particularly if the data are being used for strong-motion seismology. Figure 1 shows typical pressure sensor noise spectra in comparison with pressure amplitudes expected from typical earthquakes of varying magnitudes and distances (after Janiszewski et al., 2023). The APGs can also detect some motions from distant earthquakes and are useful for studying Rayleigh waves (e.g., Tréhu at al., 2020).

Removing Compliance Noise from Vertical Seismometer Channels

At long periods (<~0.02–0.2 Hz depending on water depth) ocean bottom seismometers are affected by noise that arises from the rotation of sensors, which results from both ocean currents and the deformation of the seafloor under surface gravity and infragravity waves. Vertical component seismometers are now routinely corrected for this noise by using the horizontal seismometer channels and a pressure gauge to predict and remove the tilt and compliance noise, respectively (Crawford and Webb, 2000; Bell et al., 2015). This can lead to noise reductions of well over an order magnitude (Bell et al., 2015; Janiszewski et al., 2023). These compliance corrections are particularly important in shallow water. SMART cables will include sensors that are buried for cable protection in shallower waters and may have a low profile above the seafloor in deeper waters. Because these configurations will be completely or partially shielded from ocean currents, compliance corrections from the pressure gauge may be the most important factor to achieve the lowest possible noise levels.

Submarine Sediment Transport Processes

Turbulent submarine sediment-laden gravity flows, known as turbidites, are an important type of sediment mass transport in the oceans. These sediment-laden flows are denser than the surrounding seawater and may produce detectable seafloor pressure changes as they pass (e.g., Arai et al., 2013; Johnson et al., 2017). Seafloor pressure data can be used in conjunction with temperature data to detect such flows to better understand the occurrence, distribution, magnitude, and frequency of these phenomena. Seafloor pressure changes due to passing turbidite flows can be on the order of 10–100 Pa (Arai et al., 2013; Johnson et al., 2017) and have durations of days to a couple of months.

Global Geodetic Observing System

Measuring the motion of mass around the earth system is the primary aim of GRACE and similar successor satellite missions. This is central to our understanding of hydrology and of the component of sea level change that is due to exchange of water between the ocean and other reservoirs such as land ice. However, GRACE is not sensitive to interhemispheric mass exchange as reflected in motion of the geocenter, therefore, complementary information is needed to constrain this part of the system. Knowledge of ocean bottom pressure variations can provide this constraint (Swenson et al., 2008). In addition, bottom pressure reflects modes of basin scale mass variations that excite variations in earth rotation (e.g., Afroosa et al., 2021; Börger et al., 2025). A network of bottom pressure recorders provides information that helps to constrain these global modes of planetary motion and contributes to implementing a precise International Terrestrial Reference Frame, which has a wide range of applications in precise navigation and satellite systems, as shown in the justification for the Genesis geodetic satellite system described here https://www.esa.int/Applications/Satellite_navigation/Genesis.

Table 2. Pressure sensing requirements for the different applications discussed (10 Pa ≅ 1 mm water)

Application	Tsunami	Oceanography	Geodesy	Seismology	Submarine sediment transport
Required sample rate	1 Hz	1 Hz	1 Hz (coseismic) to hourly	40–100 Hz	1 Hz
Required resolution	10 Pa	10 Pa	<10 Pa	≤~10 dB re 1 (Pa2/Hz) from 0.003–0.2 Hz	<10 Pa
Benefit from A-0-A drift correction?	No	Yes	Yes	No	No
Duration of signals	minutes to hours	minutes to decades	seconds to decades	seconds to minutes	minutes to weeks
Expected amplitude of signals	10 to >10,000 Pa (mm to meters sea level change)	10 to >10,000 Pa	10 to >10,000 Pa (mm to meters vertical deformation)	≥~1 Pa	10–100 Pa

SMART Cable Specifications and Recommendations for Seismic Sensors

The ground motion sensors deployed in the SMART sensing package on telecommunications cables will measure either the velocity or acceleration of the seafloor. Accelerometers are usually configured to measure strong motions while seismometers are designed to measure weak motions with self-noise levels ideally below ambient Earth noise. When deployed in SMART cables, these sensors will have a variety of potential objectives.

1. Detecting and characterizing strong offshore earthquakes to support earthquake early warning.
2. Detecting and characterizing strong offshore earthquakes and seafloor displacements to support tsunami forecasts.
3. Monitoring teleseismic earthquakes to improve the quality of global earthquake catalogs and image the internal structure of the Earth.
4. Monitoring regional earthquakes to improve earthquake catalogs, study deformation at plate boundaries, and image subsurface structure.
5. Monitoring small local microearthquakes associated with features such as volcanoes and shallow faults at oceanic plate boundaries. Repeating earthquakes can be used to study creep and other transient phenomena at plate boundaries as well as the reaction of faults to tidal and seismic forcing.
6. Studying non-volcanic tremors, which are a signal often associated with slow slip on faults.
7. Recording background noise for the purposes of ambient noise tomography and monitoring temporal changes in velocity structure.
8. Interpreting ground motion in terms of seismic wave propagation and site response/effects on the seafloor for the purposes of understanding near surface sedimentary and tectonic processes, and assessing slope stabilities during large earthquakes.
9. Measuring changes in the tilt of the seafloor related to the slumping of unstable slopes and fault motion.
10. In the absence of hydrophones, recording acoustic signals propagating in the water column, which are generated by a variety of sources including whales and other animals, earthquake T-phases and ships.

The required (and desirable) specifications for each objective are often different. Because it is envisioned that each SMART cable installation will identify and potentially prioritize a customized subset of these objectives, it is important to consider each separately.

Background

Seismic observations in the oceans are inherently limited by background noise levels (Webb, 1998). The most prominent feature of seismic noise in the oceans is the secondary microseism band that extends from 0.1–5 Hz. Secondary microseisms are generated by a non-linear interaction between surface gravity waves propagating in different directions that leads to seismic noise at double their frequency. Low frequency microseisms propagate efficiently around the Earth as Rayleigh and Love waves leading to a global peak in noise levels at ~0.15 Hz. Microseisms at frequencies ≥ ~0.5 Hz are generated locally and tend to reach saturation amplitudes at all but the lowest wind speeds. In shallow waters (< 500 m), a second peak in noise at 0.05–0.1 Hz, termed primary microseisms, consists of seismic surface waves generated by ocean swell interacting with bathymetry. Above the microseismic band, noise in the oceans results from waves breaking on coastlines and white caps, shipping, and other anthropogenic noise sources, and, seasonally, fin and blue whales. Below 0.03 Hz, noise levels in deep waters rise due to direct loading of infragravity waves, which are long period surface gravity waves with amplitudes of ≤~1 cm whose pressure variations extend to the seafloor. This leads to a noise notch at ~0.03–0.1 Hz with low noise levels except in shallow waters where seafloor deformation due to wave loading is observed in the band. At very long periods, (> 300s) seafloor noise is usually controlled by instrumental noise, often due to tilting of the sensor. Indeed, for some instrument designs, tilt noise can be a dominant source of noise up to the secondary microseism band at 10 s (Crawford and Webb, 2000; Bell et al., 2015; Janiszewski et al., 2023).

Seismic noise is typically referenced to the new low noise model (NLNM) and high noise model (NHNM), which were constructed to bracket noise spectra from 10^{-5}–10 Hz obtained from a worldwide survey of terrestrial stations, including a few on volcanic islands (Peterson, 1993).Because the dominant sources of seismic noise are within the oceans, oceanic sites tend to be noisy, particularly at frequencies below 1 Hz (Janiszewski et al., 2023, Figure 2a-b), although there are significant regional variations dependent on climate and geography (Ardhuin et al., 2011). Noise levels in the microseism band tend to be high, particularly at higher latitudes, because microseisms are generated in the oceans. In addition, at frequencies below ~0.1 Hz, the combination of pressure variations from infragravity surface waves, which deform the seafloor, and ocean currents, which rock seismometers that are not buried or shielded, leads to high noise levels. On the vertical channel, noise levels in the microseism band and below can be reduced by up to ~20 dB (Figure 2c-d) by subtracting the signals that are coherent with pressure and the tilt measured on horizontal seismometers (Crawford and Webb, 2000) but the horizontal channels remain noisy, typically above the NHNM (Figure 2b).

The seismic amplitudes of earthquakes are dependent on the size of the earthquake, geometry and pattern of fault rupture, and propagation through the Earth.Clinton and Heaton (2002) compiled an earthquake database that was used to estimate the power spectra of peak accelerations of local (10 km range), regional (100 km), and teleseismic (3000 km) earthquakes as a function of magnitude. These can be compared to seafloor noise levels (Figure 3).

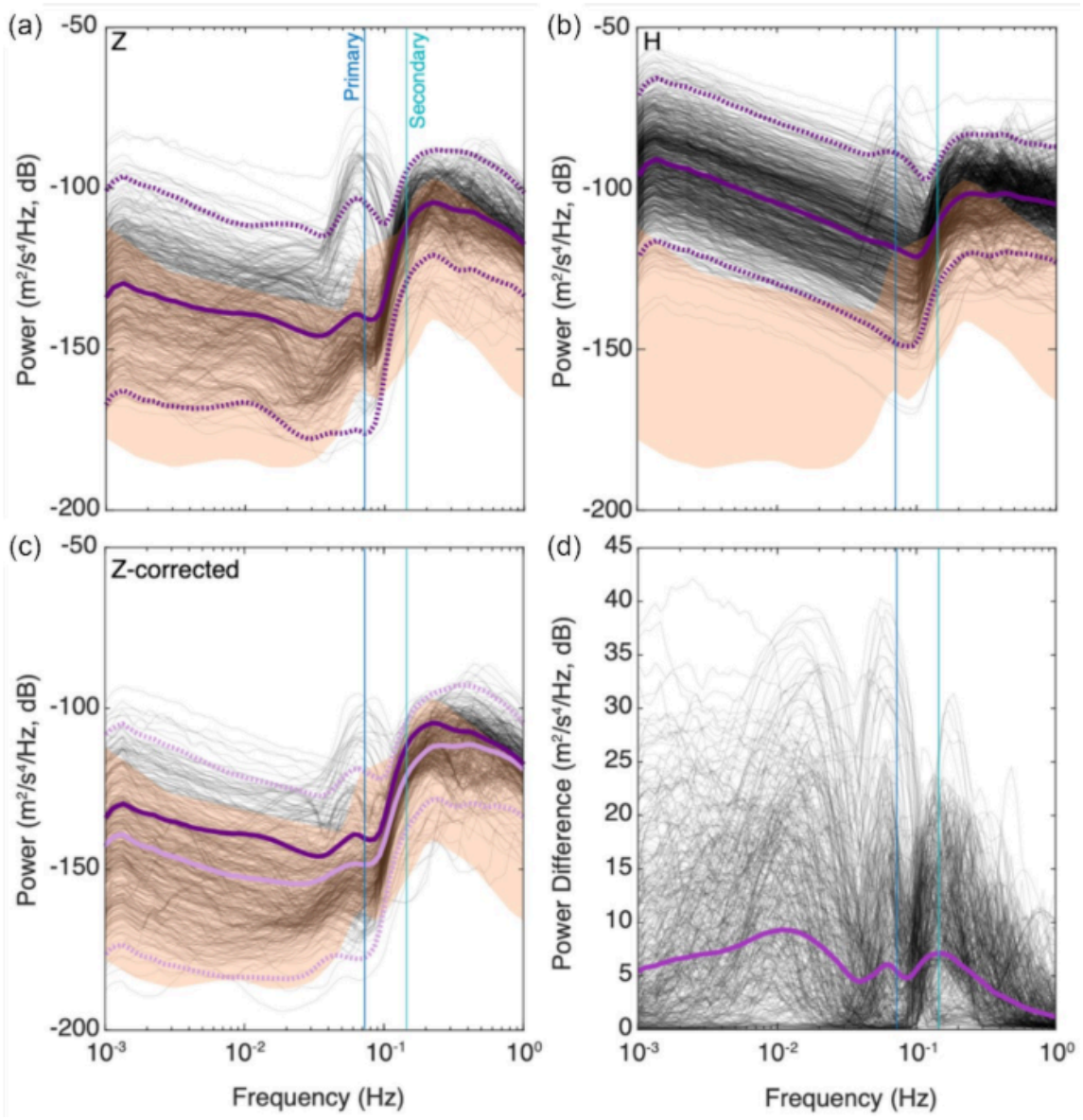

Figure 2. Compilation of noise power spectra for acceleration measured by broadband OBSs reproduced from Figure 3 of Janiszewski et al. (2023). The OBSs were deployed by the US Ocean Bottom Seismograph Instrument Pool (OBSIP) and the Ocean Bottom Seismic Instrument Center (OBSIC) with most sites in the Pacific Ocean. Power spectra for (a) the vertical channel, (b) horizontal channels, (c) the vertical channel after applying tilt- and compliance-corrections (Crawford and Webb 2000), and (d) the difference between the uncorrected and corrected vertical channel.Thin black lines show individual spectra, tan shading show the new low noise model (NLNM) and high noise model (NHNM) (Peterson, 1993), and vertical lines the peak frequency of primary and secondary microseisms. For (a) and (b), solid and dashed dark purple lines show the mean and two standard deviation limits of the spectra. In (c) the mean and two standard deviation limits are shown by pink lines with a dark purple line showing the mean for uncorrected spectra.In (d), the purple line shows the mean difference between uncorrected and corrected spectra.

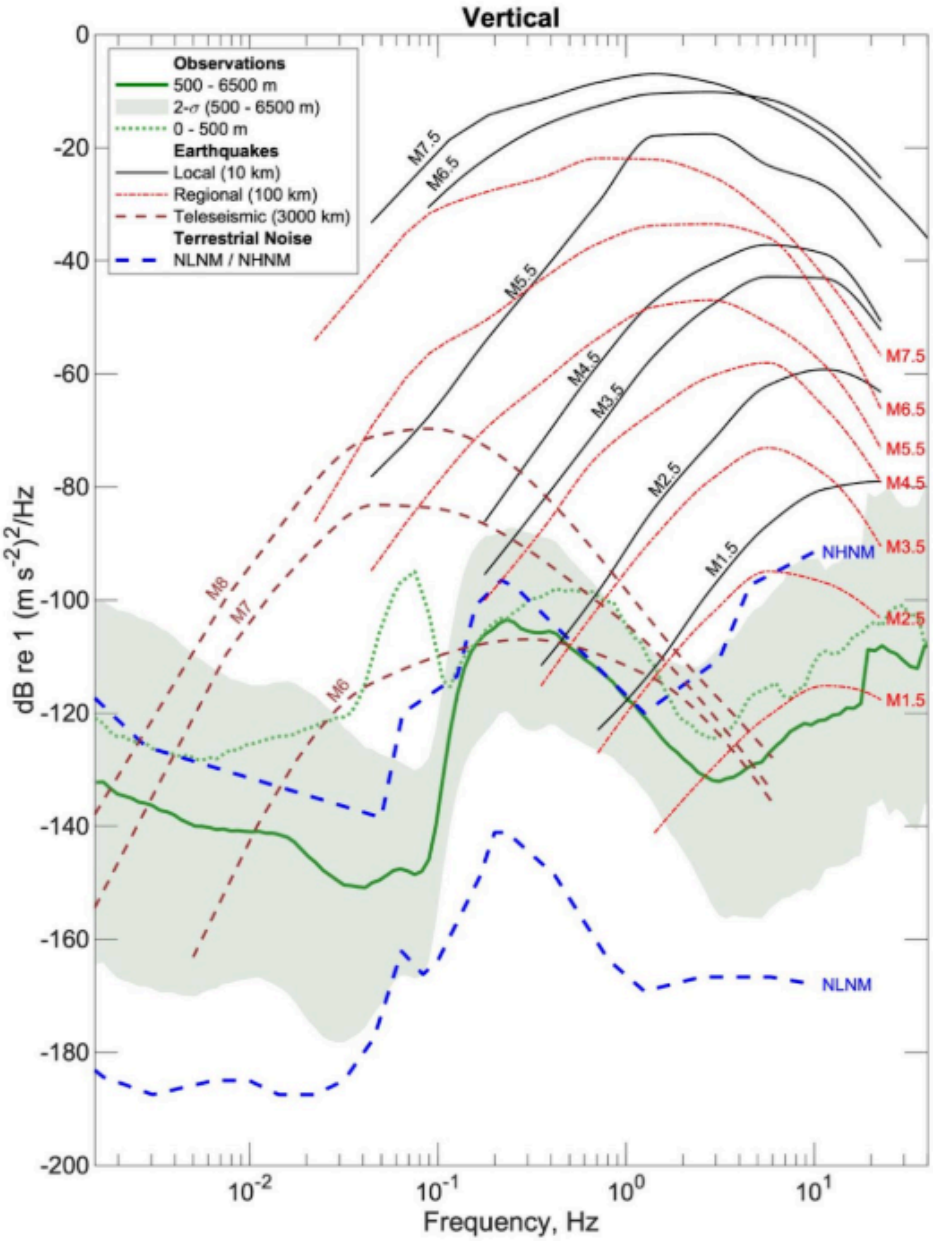

Figure 3. Vertical acceleration noise spectra compared with the power in peak accelerations of typical earthquakes in octave frequency bands. Noise spectra show the mean and two standard deviation limits at depths of 500–6500 m (solid green line and shading) and the mean at depths <500 m (dotted green) from the compilation of Janiszewski et al. (2023). Peak accelerations for earthquakes are from Clinton and Heaton (2002) and show local earthquakes at 10 km distance (red dot-dashed), regional earthquakes at 100 km (black solid) and teleseismic earthquakes at 1000 km (brown dashed) for various magnitudes. The new low and high noise models (Peterson, 1993) are also shown (blue dashed lines).

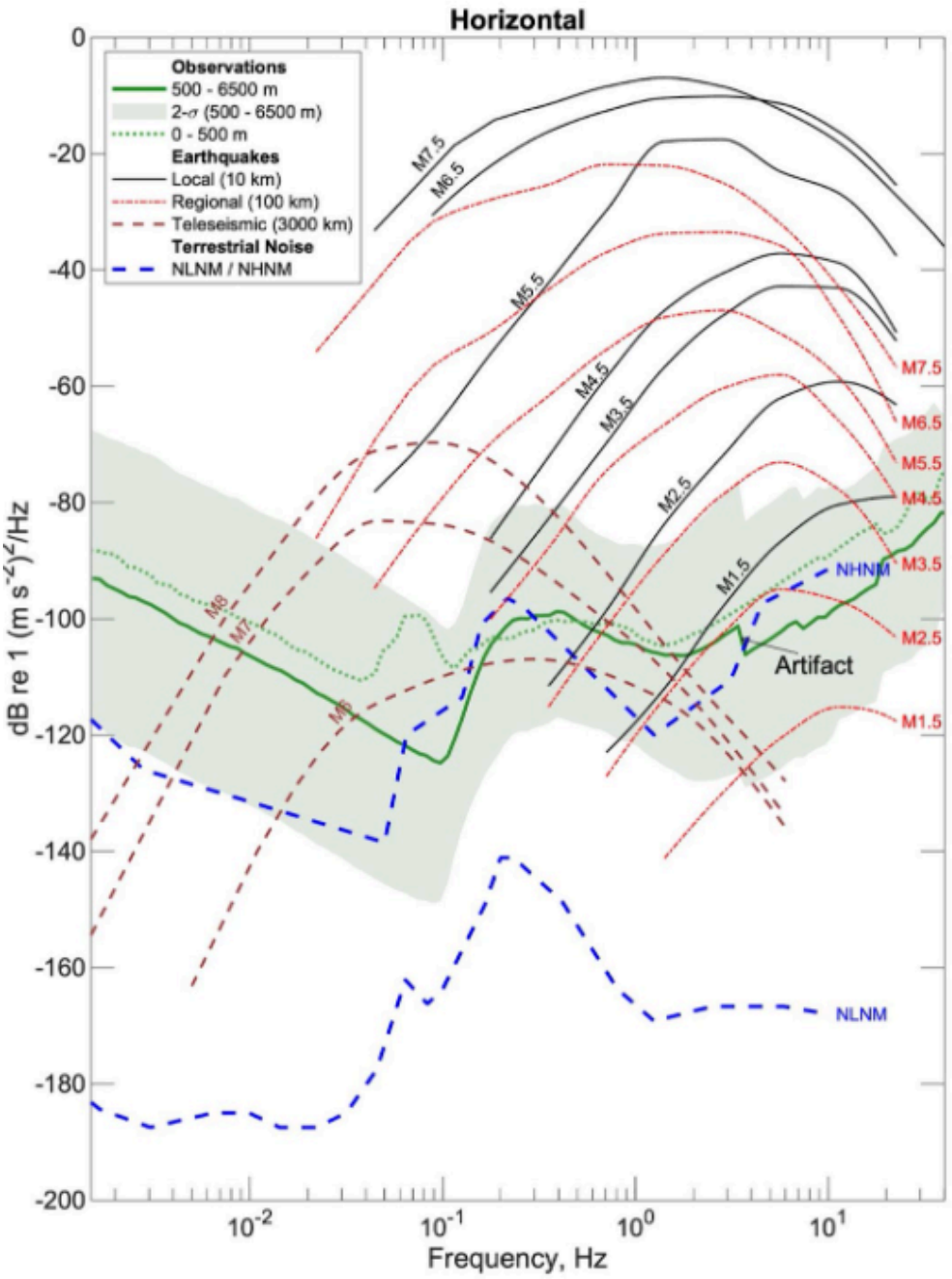

Figure 4. As in Figure 3 except for horizontal acceleration noise spectra. A step in the mean spectra at 4 Hz is an artifact of merging data with different sampling rates.

Seismic Objectives

1. Earthquake Early Warning

Earthquake early warning detects the P waves with sensors near the earthquake epicenter and, after quickly determining that an earthquake is sufficiently large, provides a short warning for the arrival of damaging S waves and surface waves at locations that are sufficiently distant from the earthquake (Kohler et al., 2020). Early warning can be used both to trigger automated responses (e.g., shutting valves on pipelines, slowing trains, opening firehouse doors) and warn the public to “drop, cover, and hold on”. Because the largest earthquakes in subduction zones nucleate offshore, there is a value to both timeliness and accuracy by detecting and characterizing these earthquakes offshore.

It is important that sensors used for early warning do not go off scale, which is typically accomplished with accelerometers that can measure accelerations well above 1-g. Because early warning is required only for earthquakes that generate strong ground motions, the requirements are not exacting in terms of sensor noise floors, although smaller earthquakes are useful for the development and verification of early warning protocols. The US ShakeAlert system utilizes frequencies >0.077 Hz (13 s period) (Kohler et al., 2020).

2. Tsunami Forecasting

For tsunamis, seismic sensors can contribute to efforts to obtain or estimate the generative seafloor displacements. Well away from the earthquake source region, seismic observations enable rapid centroid moment tensor solutions (Duputel et al., 2012) that can be combined with knowledge of fault geometries to predict likely seafloor displacements and identify potentially tsunamigenic earthquakes. These solutions are obtained at long periods (0.001–0.01 Hz), which are challenging to obtain in the oceans.

The inversion of seismic waveforms at frequencies of ~0.01–1 Hz for the detailed spatial and temporal distribution of slip is a routine tool in seismology that can use both far field data and near field strong motion data (Hartzell and Heaton, 1983).The inversions can be augmented by terrestrial high rate GNSS data (Delouis et al., 2010). For tsunami forecasts, the fault slip models obtained quickly after an earthquake can then be combined with precomputed calculations of the tsunami produced by slip on discrete blocks of subduction zone faults (Weinstein and Lundgren, 2008). Strong motion offshore observations offshore contribute to slip inversions.

In the tsunami source region, accelerometer data could, in principle, be used to measure the causative vertical ground displacement directly by twice integrating their output but such calculations are prone to large errors, which can result from integrating offsets in the baseline acceleration (Boore and Bommer, 2005).These challenges can be addressed with 6-component accelerometers to distinguish rotational from linear accelerations. On land, displacements can also be obtained by applying a Kalman filter to the combination of accelerometer and high-rate GNSS data (Bock et al., 2011). A similar approach may be feasible on the seafloor with the combination of bottom pressure and acceleration observations (Mizutani et al., 2024).

Kubota et al. (2021) demonstrate using the dynamic signal caused by uplift observed with pressure gauges to estimate seafloor displacements in the source region of a tsunami. Kozdon and Dunham (2013) describe using pressure or seismometer observation of near source acoustic waves to estimate tsunami source region displacements.

3. Global Seismology

Teleseismic earthquakes are observed at frequencies that range from < 0.01 Hz to a few hertz. The lack of observations in the oceans substantially degrades images of the Earth structure and the completeness of global earthquake catalogs. Frequencies of 1 Hz to a few hertz are important for recording compressional body waves, while the low noise notch at frequencies of 0.03–0.1 Hz is used for surface and S waves. Teleseismic body waves are also regularly used in the low noise notch to study local structure through the use of receiver functions to identify subsurface interfaces (Janiszewski and Abers, 2015) and shear wave splitting to understand anisotropy related to mantle flow (Bodmer et al., 2015).

The self-noise of broadband seismometers deployed to monitor teleseismic earthquakes in terrestrial settings is typically specified below NLNM (Peterson, 1993). Because the oceans are noisy, the NLMN is too exacting a requirement for most seafloor sites (Figures 2a-b). However, instrument noise levels should be low enough so as not to obscure the low noise notch and also take into account geographic variations in noise. If the vertical channel is corrected for tilt and compliance using horizontal channels and pressure recordings, vertical noise levels can be markedly reduced (Figure 2c). At frequencies of 1 to a few Hz, noise levels can drop by ~15 dB between wind speeds of 20 knots (10 m/s) and calm (Wilcock et al., 2021). Geography and climate are important considerations for specifying the required noise floor (Webb, 1998).

Based on the compilation of Janiszewski et al. (2023), self-noise levels on the vertical channel in the low noise notch of -145 dB and -170 dB re 1 $(m\ s^{-2})^2$/Hz would be required to match the mean and lower two standard deviation (2-σ) ambient noise levels for the vertical channel (Figure 2a, 3). For tilt and compliance-corrected vertical channel data, these thresholds are lowered to -155 dB and -180 dB, respectively (Figure 2c). In contrast, a self-noise level on the horizontal channel of -150 dB would match the lower 2-σ ambient noise levels (Figure 2b, 4). For frequencies of 1–4 Hz, the mean and lower 2-σ ambient noise levels are -130 dB and-155 dB, respectively (Figure 3).However, burial of the OBS sensor may significantly reduce noise on the horizontal channel (Stephen et al., 2003).Because SMART cables are likely to be buried in shallow water, the self-noise specifications for horizontal channels are best set to match those for the vertical channel.

4. Regional Earthquakes

and in tectonically active areas will require observations that are sensitive to both strong and weak motions. In subduction zones, terrestrial and seafloor data are often combined to study regional earthquakes.Regional earthquake observations can be used to locate earthquakes, estimate source parameters using moment tensor inversions (Pasyanos et al., 1996), and image subsurface structure (Byrnes et al., 2017; Lange et al., 2018; Janiszewski et al., 2019; Arnulf et al., 2022).

5. Local Microearthquakes

Studies of microearthquakes at ocean spreading centers, transform faults, and submarine volcanoes are typically conducted with networks of seismometers recording signals at 1–100 Hz, which are spaced a few kilometers apart. Thus, they may not be well suited for SMART cables although there are techniques to characterize seismicity using a single station that could be applied to both local and regional earthquakes (Magotra et al., 1987; Böse et al., 2017)

6. Non-Volcanic Tremor

In subduction zones, offshore seismic observations can be used to search for shallow tectonic tremors, which are indicative of slow slip on the megathrust. Tremors are typically observed at ~3–12 Hz. Tectonic tremors have been observed with ocean bottom seismometers off New Zealand (Wech et al., 2013; Todd et al., 2018) and Japan (Yamashita et al., 2021).

7. Ambient Noise

Cross-correlation techniques can be applied to the ambient noise recorded on two seismometers to estimate the seismic signal that would be recorded on one seismometer for an impulsive source at the other (i.e., Green's function). When the technique is applied to an array of seismometers, the method can provide a data set of surface waves that can be inverted at frequencies of 0.02–0.2 Hz for subsurface structure (Porritt et al., 2011; Ritzwoller et al., 2011; Gao and Shen, 2015). Noise cross-correlation between stations or between channels on the same station can be applied to monitor for temporal changes in the Green's function resulting from small changes in seismic speed caused by tectonic deformation or other processes that modulate seismic velocities (Campillo and Roux, 2015). For stations spaced at 50–100 km in the oceans, which is the typical spacing of repeaters on SMART cables, such monitoring may be feasible up to 1 Hz (Chaves and Schwartz, 2016). Measurements are typically obtained from 0.1 Hz to ~4 Hz when analyzing single stations (De Plaen et al., 2016).

8. Ground Motion

Understanding the causes and impacts of ground motions from earthquakes requires both theoretical modeling and empirical observations.Even onshore ground motion parameters are observed to be highly variable, and depend on source, path, and site effects (Douglas and Edwards, 2016). Empirical constraints on ground motions rely on data provided by distributions of sensors (Gomberg, 2018). Wave propagation can be modeled using noise cross-correlations of long continuous recordings. Sensors in different site conditions can lead to an understanding of site response and effects. It is difficult to identify any specific requirements for these purposes. As a broad generalization, these sensors should have a wide dynamic range in order to record the signals of small local earthquakes and remain on-scale if strongly shaken. They should also detect ambient ground motions at frequencies of about 0.1–50 Hz.

9. Tilt

A horizontal accelerometer with a response down to DC (0 Hz) can be used as a tiltmeter. In SMART cables it has potential value for measuring the settling of the sensors, slope stability, and geodetic signals such as slow slip events. Sensor settling and slope stability can be observed with tiltmeters with a stability of 100 μrad per year (García et al., 2010; Wilcock et al., 2021), however, geodetic observations require a stability of ~1 μrad per year and precision of ~0.01 μrad (Ito et al., 2007)

10. Ocean Acoustic

Seismometers are sensitive to acoustic signals up to at least 100 Hz. They can be used to study the low frequency calls of baleen whales (fin, blue, Bryde, sei, humpback) (McDonald et al., 1995) and also record ships (Trabattoni et al., 2020). T-phases are earthquake waves with frequencies up to tens of hertz that travel through the water column and can be observed with hydrophones or seafloor seismometers. They carry information about both ocean acoustics and seafloor properties, and have been used to characterize ocean temperature (Wu et al., 2020) and earthquake, volcano, and landslide sources (Okal, 2008). Thus, a seismic sensor on a SMART cable might serve as a useful alternative or complement to a low-frequency hydrophone.

Specifications

Application	EEW, Strong Motion Seismology	Teleseismic Earthquakes	Regional Seismology	Microearthquakes Ocean Acoustics	Tilt
Application	1, 2, 4, 8	3	4, 6, 7, 8	5, 10	9
Components (V - Vertical, H - Horizontals)	V, H	V, H	V, H	V, H Mainly V for acoustics	H
Frequency Band	0.0833–50 Hz	0.003–4 Hz	0.03–20 Hz	1–100 Hz (or higher for acoustics)	0 Hz
Self-noise (re 1 (m/s2)2/Hz)	-120 dB	-155 dB to -180 dB at 0.03-0.1 Hz-130 dB to -155 dB at 1-4 Hz	As for teleseismic	-155 dB at 1-10 Hz	
Other	Full Scale >1 g				Stability 100 μrad/yr to ≤1μrad/yr
Minimum sample rate	100 Hz	8 Hz	40 Hz	200 Hz (or more for acoustics)	<<1 Hz

Future Developments

Differential Pressure Gauges

Except in shallow settings where the pressure signals from surface gravity waves are large, the absolute pressure gauges envisioned for SMART cables sensor packages may not always have low enough noise levels at the frequencies of interest to allow optimal corrections for compliance noise. Adding a differential pressure gauge (DPG; Cox et al., 1984) to the SMART sensor package could improve the quality of vertical seismic data in deep water by enabling the removal of noise due to deformation under the loading of infragravity waves (compliance noise; Webb and Crawford, 2010).

Horizontal Pressure Gradients

Corrections of horizontal channels for tilt noise from ocean surface gravity and infragravity waves would be possible with measurements of horizontal pressure gradient across the sensor (Webb and Barclay, 2023).

Rotational Sensors

Within tsunami source regions, measurements for seafloor vertical displacement would provide the most direct means to predict the tsunami.Obtaining displacements by double integrating acceleration data is challenging because baseline offsets and rotation on the sensor can lead to large errors in the integrations. On land, accelerometer and high rate GNSS data can be combined to obtain good estimates of displacement (Emore et al., 2007).In the oceans, six component acceleration data for a combined linear and rotational accelerometer would enable such calculations.

References

Afroosa, M., Rohith, B., Paul, A. et al. (2021). Madden-Julian oscillation winds excite an intraseasonal see-saw of ocean mass that affects Earth's polar motion. Commun. Earth Environ. 2:139. https://doi.org/10.1038/s43247-021-00210-x

Aoi, S., Asano, Y., Kunugi, T. et al. (2020). MOWLAS: NIED observation network for earthquake, tsunami and volcano. Earth Planets Space 72:126. doi:10.1186/s40623-020-01250-x.

Aoki, Y., and Scholz, C.H. (2003). Vertical deformation of the Japanese islands, 1996–1999. J. Geophys. Res. Solid Earth, 108(B5).

Arai, K., Naruse, H., Miura, R., Kawamura, K., Hino, R., Ito, Y., et al. (2013). Tsunami-generated turbidity current of the 2011 Tohoku-Oki earthquake. Geology 41(11):1195–1198.

Ardhuin, F., Stutzmann, E., Schimmel, M., and Mangeney, A. (2011). Ocean wave sources of seismic noise. J. Geophys. Res. Oceans, 116(C9).

Arnulf, A. F., Bassett, D., Harding, A. J., Kodaira, S., Nakanishi, A., and Moore, G. (2022). Upper-plate controls on subduction zone geometry, hydration and earthquake behaviour. Nat. Geosci., 15(2):143–148.

Bell, S. W., Forsyth, D. W., and Ruan, Y. (2015). Removing noise from the vertical component records of ocean-bottom seismometers: Results from year one of the Cascadia Initiative. Bull. Seismol. Soc. Am., 105(1):300–313.

Bernard, E., Wei, Y., Tang, L., and Titov, V. (2014). Impact of near-field, deep-ocean tsunami observations on forecasting the 7 December 2012 Japanese tsunami. Pure Appl. Geophys. 171(12):3483–3491. doi:10.1007/s00024-013-0720-8.

Bock, Y., Melgar, D., and Crowell, B. W. (2011). Real-time strong-motion broadband displacements from collocated GPS and accelerometers. Bull. Seismol. Soc. Am., 101(6), 2904–2925. https://doi.org/10.1785/0120110007.

Bodmer, M., Toomey, D. R., Hooft, E. E., Nábělek, J., and Braunmiller, J. (2015). Seismic anisotropy beneath the Juan de Fuca plate system: Evidence for heterogeneous mantle flow. Geology, 43(12):1095–1098.

Boore, D. M., and Bommer, J. J. (2005). Processing of strong-motion accelerograms: needs, options and consequences. Soil Dyn. Earthq. Eng. 25(2):93–115.

Börger, L., Schindelegger, M., Zhao, M., Ponte, R. M., Löcher, A., Uebbing, B., et al. (2025). Chaotic oceanic excitation of low-frequency polar motion variability. Earth Syst. Dynam. 16:75–90. https://doi.org/10.5194/esd-16-75-2025.

Böse, M., Clinton, J. F., Ceylan, S., Euchner, F., van Driel, M., Khan, A., et al. (2017). A probabilistic framework for single-station location of seismicity on Earth and Mars. Phys. Earth Planet. Int. 262:48–65.

Byrnes, J. S., Toomey, D. R., Hooft, E. E., Nábělek, J., and Braunmiller, J. (2017). Mantle dynamics beneath the discrete and diffuse plate boundaries of the Juan de Fuca plate: Results from Cascadia Initiative body wave tomography. Geochem. Geophys. Geosyst. 18(8):2906–2929.

Campillo, M., and Roux, P. (2015). “Seismic imaging and monitoring with ambient noise correlations in crust and lithospheric structure”, in Treatise on Geophysics, eds B. Romanowicz and A Dziewonski (Elsevier), Vol. 1, 391–417.
Chadwick Jr, W.W., Nooner, S.L., Zumberge, M.A., Embley, R.W. and Fox, C.G. (2006). Vertical deformation monitoring at Axial Seamount since its 1998 eruption using deep-sea pressure sensors. J. Volcanol. Geotherm. Res. 150(1-3):313–327.
Chaves, E. J., and Schwartz, S. Y. (2016). Monitoring transient changes within overpressured regions of subduction zones using ambient seismic noise. Sci. Adv. 2(1):e1501289.
Clinton, J. F., and Heaton, T. H. (2002). Potential advantages of a strong-motion velocity meter over a strong-motion accelerometer. Seismol. Res. Lett. 73(3):332–342.
Cox, C., Deaton, T., and Webb, S. (1984). A deep-sea differential pressure gauge. J. Atmos. Ocean. Technol. 1(3):237–246.
Crawford, W. C., and Webb, S. C. (2000). Identifying and removing tilt noise from low-frequency (< 0.1 Hz) seafloor vertical seismic data. Bull. Seismol. Soc. Am. 90(4):952–963.
De Plaen, R. S., Lecocq, T., Caudron, C., Ferrazzini, V., and Francis, O. (2016). Single-station monitoring of volcanoes using seismic ambient noise. Geophys. Res. Lett. 43(16):8511–8518.
Delouis, B., Nocquet, J. M., and Vallée, M. (2010). Slip distribution of the February 27, 2010 Mw= 8.8 Maule earthquake, central Chile, from static and high-rate GPS, InSAR, and broadband teleseismic data. Geophys. Res. Lett. 37(17).
Douglas, J., and Edwards, B. (2016). Recent and future developments in earthquake ground motion estimation. Earth-Sci. Rev. 160:203-219.
Duputel, Z., Rivera, L., Kanamori, H., and Hayes, G. (2012). W phase source inversion for moderate to large earthquakes (1990–2010). Geophys. J. Int. 189(2):1125–1147.
Emore, G. L., Haase, J. S., Choi, K., Larson, K. M., and Yamagiwa, A. (2007). Recovering seismic displacements through combined use of 1-Hz GPS and strong-motion accelerometers. Bull. Seismol. Soc. Am. 97(2):357–378.
Filloux, J. H. (1983). Pressure fluctuations on the open-ocean floor off the Gulf of California: Tides, earthquakes, tsunamis. J. Phys. Oceanogr. 13:783–796. doi:10.1175/1520-0485(1983)013<0783:PFOTOO>2.0.CO;2.
Fujii, Y., and Satake, K. (2024). Modeling the 2022 Tonga eruption tsunami recorded on ocean bottom pressure and tide gauges around the Pacific. Pure Appl. Geophys. doi:10.1007/s00024-024-03477-1.
Fukao, Y., Sandanbata, O., Sugioka, H., Ito, A., Shiobara, H., Watada, S., et al. (2018). Mechanism of the 2015 volcanic tsunami earthquake near Torishima, Japan. Sci. Adv. 4:eaao0219. doi:10.1126/sciadv.aao0219.
García, A., Hördt, A., and Fabian, M. (2010). Landslide monitoring with high resolution tilt measurements at the Dollendorfer Hardt landslide, Germany. Geomorph. 120(1-2):16–25.

Gomberg, J. (2018). Cascadia onshore-offshore site response, submarine sediment mobilization, and earthquake recurrence. J. Geophys. Res. Solid Earth 123(2):1381–1404.
Hartzell, S. H., and Heaton, T. H. (1983). Inversion of strong ground motion and teleseismic waveform data for the fault rupture history of the 1979 Imperial Valley, California, earthquake. Bull. Seismol. Soc. Am., 73(6A):1553–1583.
Herrford, J., Brandt, P., and Zenk, W. (2017). Property changes of deep and bottom waters in the western tropical Atlantic. Deep-Sea Res. I 124:103–125. doi:10.1016/j.dsr.2017.04.007.
Herrford, J., Brandt, P., Kanzow, T., Hummels, R., Araujo, M., and Durgadoo, J. V. (2021). Seasonal variability of the Atlantic Meridional Overturning Circulation at 11° S inferred from bottom pressure measurements. Ocean Sci. 17:265–284. doi:10.5194/os-17-265-2021.
Houston, M.H., and Paros J.M. (1998). "High accuracy pressure instrumentation for underwater applications", in Proceedings of the 1998 International Symposium on Underwater Technology, IEEE, 307–311, doi:10.1109/UT.1998.670113.
Hughes, C. W., Tamisiea, M.E., Bingham, R.J., and Williams, J. (2012). Weighing the ocean: Using a single mooring to measure changes in the mass of the ocean. Geophys. Res. Lett. 39(17):L17602. doi: 10.1029/2012GL052935.
Hughes, C.W., Williams, J., Blaker, A., Coward, A. and Stepanov, V. (2018). A window on the deep ocean: the special value of ocean bottom pressure for monitoring the large-scale, deep-ocean circulation. Progr. Oceanogr. 161:19–46.
Iinuma, T., Hino, R., Kido, M., Inazu, D., Osada, Y., Ito, Y., et al. (2012). Coseismic slip distribution of the 2011 off the Pacific Coast of Tohoku Earthquake (M9.0) refined by means of seafloor geodetic data. J. Geophys. Res. Solid Earth 117(B7):B07409. doi:10.1029/2012JB009186.
Ito, Y., Obara, K., Shiomi, K., Sekine, S., and Hirose, H. (2007). Slow earthquakes coincident with episodic tremors and slow slip events. Science 315(5811):503-506.
Janiszewski, H. A., and Abers, G. A. (2015). Imaging the plate interface in the Cascadia seismogenic zone: New constraints from offshore receiver functions. Seismol. Res. Lett. 86(5), 1261-1269.
Janiszewski, H. A., Gaherty, J. B., Abers, G. A., Gao, H., and Eilon, Z. C. (2019). Amphibious surface-wave phase-velocity measurements of the Cascadia subduction zone. Geophys. J. Int. 217(3):1929–1948.
Janiszewski, H. A., Eilon, Z., Russell, J. B., Brunsvik, B., Gaherty, J. B., Mosher, S. G., et al. (2023). Broad-band ocean bottom seismometer noise properties. Geophys. J. Int. 233(1), 297–315.
Jegen, A., Lange, D., Karstensen, J., Pizarro, O., and Kopp, H. (2024). Deep ocean hydrographic variability estimated from distributed geodetic sensor arrays off northern Chile. Sci. Rep. 14(1):11163. doi: 10.1038/s41598-024-61929-z. PMID: 38750211; PMCID: PMC11096396.
Johnson, H. P., Gomberg, J. S., Hautala, S. L., and Salmi, M. S. (2017). Sediment gravity flows triggered by remotely generated earthquake waves. J. Geophys. Res. Solid Earth 122:4584–4600. doi:10.1002/2016JB013689.
Kohler, M. D., Smith, D. E., Andrews, J., Chung, A. I., Hartog, R., Henson, I., et al. (2020). Earthquake early warning ShakeAlert 2.0: Public rollout. Seismol. Res. Lett. 91(3):1763–1775.

Körner, M., Brandt, P., Illig, S., Dengler, M., Subramaniam, A., Bachèlery, M.-L., et al. (2024). Coastal trapped waves and tidal mixing control primary production in the tropical Angolan upwelling system. Sci. Adv. 10:eadj6686. doi:10.1126/sciadv.adj6686.
Kozdon, J. E., and Dunham, E. M. (2014). Constraining shallow slip and tsunami excitation in megathrust ruptures using seismic and ocean acoustic waves recorded on ocean-bottom sensor networks. Earth and Planetary Science Letters, 396: 56-65.
Kubo, H., Kubota, T., Suzuki, W., Aoi, S., Sandanbata, O., Chikasada, N., et al. (2022). Ocean-wave phenomenon around Japan due to the 2022 Tonga eruption observed by the wide and dense ocean-bottom pressure gauge networks. Earth Planets Space 74(1):104.
Kubota, T., Kubo, H., and Saito, T. (2025). Reliable fault modeling of an Mw 7.1 earthquake in Hyuganada Sea on 8 August 2024 by offshore tsunami data from new seafloor network N-net and onshore GNSS data. Geophys. Res. Lett. 52:e2025GL115391. doi;10.1029/2025GL115391.
Kubota, T., Saito, T., Tsushima, H., Hino, R., Ohta, Y., Suzuki, S., et al. (2021). Extracting near-field seismograms from ocean-bottom pressure gauge inside the focal area: Application to the 2011 Mw 9.1 Tohoku-Oki earthquake. Geophys. Res. Lett. 48(7):e2020GL091664.
Lange, D., Tilmann, F., Henstock, T., Rietbrock, A., Natawidjaja, D., and Kopp, H. (2018). Structure of the central Sumatran subduction zone revealed by local earthquake travel-time tomography using an amphibious network. Solid Earth 9(4):1035–1049.
Maeda, T., Furumura, T., Sakai, S., and Shinohara, M. (2011). Significant tsunami observed at ocean-bottom pressure gauges during the 2011 off the Pacific coast of Tohoku Earthquake. Earth Planet Space 63:53. doi;10.5047/eps.2011.06.005.
Magotra, N., Ahmed, N., and Chael, E. (1987). Seismic event detection and source location using single-station (three-component) data. Bull. Seismol. Soc. Am. 77(3):958-971.
Matsumoto, H., and Araki, E. (2021). Drift characteristics of DONET pressure sensors determined from in-situ and experimental measurements. Front. Earth Sci. 8:600966.
Matsumoto, H., Kimura, T., Nishida, S., Machida, Y. and Araki, E. (2018). Experimental evidence characterizing pressure fluctuations at the seafloor-water interface induced by an earthquake. Sci. Rep. 8(1):16406.
McDonald, M. A., Hildebrand, J. A., and Webb, S. C. (1995). Blue and fin whales observed on a seafloor array in the Northeast Pacific. J. Acoust. Soc. Am. 98(2):712–721.
Meinen, C. S., Perez, R. C., Dong, S., Piola, A. R., and Campos, E. (2020). Observed ocean bottom temperature variability at four sites in the Northwestern Argentine basin: Evidence of decadal deep/abyssal warming amidst hourly to interannual variability during 2009–2019. Geophys. Res. Lett. 47, e2020GL089093. https://doi.org/10.1029/2020GL089093.
Mizutani, A., Melgar, D., and Yomogida, K. (2024). Strong-motion broadband displacements from collocated ocean-bottom pressure gauges and seismometers. Geophys. Res. Lett. 51:e2023GL107776. https://doi.org/10.1029/2023GL107776.
Nosov, M. A., and Kolesov, S. V. (2007). Elastic oscillations of water column in the 2003 Tokachi-oki tsunami source: in-situ measurements and 3-D numerical modelling. Nat. Hazards Earth Syst. Sci. 7:243–249. doi: 10.5194/nhess-7-243-2007.

Okal, E. A. (2008). The generation of T waves by earthquakes. Adv. Geophys. 49:1–65.
Pasyanos, M. E., Dreger, D. S., and Romanowicz, B. (1996). Toward real-time estimation of regional moment tensors. Bull. Seismol. Soc. Am. 86(5):1255–1269.
Peltier, W.R. (1999). Global sea level rise and glacial isostatic adjustment. Global Planet. Change 20(2-3):93–123.
Peterson, J. R. (1993). Observations and Modeling of Seismic Background Noise (No. 93-322). US Geological Survey.
Polster, A., Fabian, M., and Villinger, H. (2009). Effective resolution and drift of Paroscientific pressure sensors derived from long-term seafloor measurements. Geochem. Geophys. Geosyst. 10:Q08008. doi:10.1029/2009GC002532.
Porritt, R. W., Allen, R. M., Boyarko, D. C., and Brudzinski, M. R. (2011). Investigation of Cascadia segmentation with ambient noise tomography. Earth Planet. Sci. Lett. 309(1-2):67-76.
Purkey, S. G., and Johnson, G. C. (2010). Warming of global abyssal and deep Southern Ocean waters between the 1990s and 2000s: Contributions to global heat and sea level rise budgets. J. Climate 23:6336–6351.
Ray, R. D. (2013). Precise comparisons of bottom-pressure and altimetric ocean tides. J. Geophys. Res. Oceans 118(9):4570–4584. doi:10.1002/jgrc.20336.
Ritzwoller, M. H., Lin, F. C., and Shen, W. (2011). Ambient noise tomography with a large seismic array. CR Geosci. 343(8-9):558-570.
Stephen, R. A., Spiess, F. N., Collins, J. A., Hildebrand, J. A., Orcutt, J. A., Peal, K. R., et al. (2003). Ocean Seismic Network Pilot Experiment. Geochem. Geophys. Geosyst. 4(10):1092. doi:10.1029/2002GC000485.
Swenson, S., Chambers, D., and Wahr, J. (2008). Estimating geocenter variations from a combination of GRACE and ocean model output. J. Geophys. Res. 113:B08410. doi:10.1029/2007JB005338.
Todd, E. K., Schwartz, S. Y., Mochizuki, K., Wallace, L. M., Sheehan, A. F., Webb, S. C., et al. (2018). Earthquakes and tremor linked to seamount subduction during shallow slow slip at the Hikurangi margin, New Zealand. J. Geophys. Res. Solid Earth 123(8):6769–6783.
Trabattoni, A., Barruol, G., Dreo, R., Boudraa, A. O., and Fontaine, F. R. (2020). Orienting and locating ocean-bottom seismometers from ship noise analysis. Geophys. J. Int. 220(3):1774–1790.
Tréhu, A. M., de Moor, A., Mieres Madrid, J., Sáez, M., Chadwell, C. D., Ortega-Culaciati, F., et al. (2020). Post-seismic response of the outer accretionary prism after the 2010 Maule earthquake, Chile. Geosphere 16(1):13-32.
Wallace, L.M., Webb, S. C., Ito, Y., Mochizuki, K., Hino, R., Henrys, S., et al. (2016). Slow slip near the trench at the Hikurangi subduction zone. Science 352(6286):701-704. doi: 10.1126/science.aaf2349.
Webb, S. C. (1998). Broadband seismology and noise under the ocean. Rev. Geophys. 36(1):105–142.
Webb, S. C., and Barclay, A. H. (2023). Optimizing ocean bottom seismometers for shallow water using shielding and horizontal pressure gradient data. J. Geophys. Res. Solid Earth 128:e2023JB026356.
Webb, S.C., and Crawford, W.C. (2010). Shallow water broad band OBS seismology. Bull. Seismol. Soc. Am. 100(4):1770-1778. doi: 10.1785/012009020.

Webb, S.C.W, and Nooner, S. (2016). High-resolution seafloor absolute pressure gauge measurements using a better counting method. J. Atmos. Ocean. Technol. 33(9):1859-1874. https://doi.org/10.1175/JTECH-D-15-0114.1

Wech, A. G., Sheehan, A. F., Boese, C. M., Townend, J., Stern, T. A., and Collins, J. A. (2013). Tectonic tremor recorded by ocean bottom seismometers. Seismol. Res. Lett. 84(5):752-758.

Weinstein, S. A., and Lundgren, P. R. (2008). Finite fault modeling in a tsunami warning center context. Pure Appl. Geophys. 165:451–474.

Wilcock, W. S. D., Manalang, D. A., Fredrickson, E. K., Harrington, M. J., Cram, G., Tilley, J., et al. (2021). A thirty-month seafloor test of the A-0-A method for calibrating pressure gauges. Front. Earth Sci. 8:653. https://doi.org/10.3389/feart.2020.600671.

Williams, J., Hughes, C. W., Tamisiea, M. E., and Williams, S. D. P. (2014). Weighing the ocean with bottom-pressure sensors: robustness of the ocean mass annual cycle estimate. Ocean Sci. 10:701–718. doi: 10.5194/os-10-701-2014.

Woods, K., Webb, S.C., Wallace, L.M., Ito, Y., Collins, C., Palmer, N., Hino, R., et al. (2022). Using seafloor geodesy to detect vertical deformation at the Hikurangi subduction zone: Insights from self-calibrating pressure sensors and ocean general circulation models. J. Geophys. Res. Solid Earth 127(12):e2022JB023989.

Wu, W., Zhan, Z., Peng, S., Ni, S., and Callies, J. (2020). Seismic ocean thermometry. Science 369(6510):1510–1515. https://doi.org/10.1126/science.abb9519.

Yamashita, Y., Shinohara, M., and Yamada, T. (2021). Shallow tectonic tremor activities in Hyuga-nada, Nankai subduction zone, based on long-term broadband ocean bottom seismic observations. Earth Planet. Space 73:1–11.

Zhou, S., Meijers, A.J.S., Meredith, M.P. et al. (2023). Slowdown of Antarctic bottom water export driven by climatic wind and sea-ice changes. Nat. Clim. Change 13:701–709. doi: 10.1038/s41558-023-01695-4.

SMART CABLES

Connecting Humanity,
Understanding the Earth.